Polymer Chemistry

ARTICLE

Non-steady Scaling Model for the Free Radical Polymerization Kinetics of Crosslinked Networks

Received 00th January 20xx,
Accepted 00th January 20xx

DOI: 10.1039/x0xx00000x
www.rsc.org/

Patrice Roose,*[a] Evelien Vermoesen [b] and Sandra Van Vlierberghe [b]

Recently, a semi-empirical scaling model was introduced to account for the free-radical polymerization kinetics of acrylated urethane precursors in the solid-state. By describing the radical initiation process in more detail, the kinetic model is extended herein towards general free-radical crosslinking irrespective of the initial physical state of the multifunctional precursors. Effects referred to as radical trapping and caging in literature are clearly specified and a closed-form expression with a limited number of adjustable parameters is obtained which can be compared to experimental kinetics. In particular, the relation between polymerization rate and functional conversion can be reduced to expressions with three and four parameters in the limits of "solid-state" and "steady-state" kinetics, respectively. In the case of photo-induced free-radical polymerization and within the slow decomposition regime of the initiator, the single parameter with an explicit dependence on the incident light intensity is predicted to behave proportionally. The model is validated by comparing the relevant expressions to original calorimetric data for the free-radical photopolymerization kinetics of different acrylate urethane precursors at two temperatures, providing illustrations for solid-to-solid and liquid-to-rubber transformations. Careful monitoring of the effect of light intensity corroborates the expected scaling and additionally offers reliable estimates for the kinetic coefficients of propagation and termination.

.

Introduction

The complexity behind the polymerization kinetics of free-radical chain processes stems primarily from the structural changes of the radical- and functional-bearing molecular entities, affecting their accessibility and the respective kinetic rate coefficients. The subject has been investigated over many decades but there is still a need for useful models which can approximate kinetic data over the entire conversion range, in particular for crosslinking polymerizations.[1-21] As an example, kinetic data obtained from differential photocalorimetry or time-resolved FTIR spectroscopy are often used to appreciate the efficiency of photo-initiators during the photopolymerization of multifunctional precursors. In this case, the maximum polymerization rate is usually considered as a relevant quantitative metric although it involves all the kinetic events and is not related to initiation efficiency in a straightforward way.[22,23] Kinetic studies could benefit from appropriate models to resolve the polymerization process in sufficient detail and avoid ambiguous conclusions.

In a preceding paper, we outlined a semi-empirical approach based on scaling principles to account for the free-radical polymerization kinetics of multiacrylates in an immobile semi-crystalline state.[24] Building on established understanding, a closed-form mathematical expression was derived for the polymerization rate in terms of the fractional conversion, taking into account the structural effects controlling the kinetic coefficients and non-steady state (transient) behaviour. Comparison to experimental data showed that the model describes the overall phenomenology successfully with a limited number of adjustable parameters which can be rationalized in terms of the rate coefficients of initiation, propagation and termination. In the case of photo-activation, the single parameter depending on the incident light intensity predicts a first-order behaviour which could not be established properly so far. Furthermore, the effects of trapping and caging of radicals were not distinctly captured in the model and still lack some clarity. By expanding on the radical initiation mechanism in this paper, it is demonstrated that a coherent picture emerges with minor, yet important

[a] *allnex Belgium SA/NV, Anderlechtstraat 33, Drogenbos, B-1620, Belgium*
[b] *Polymer Chemistry & Biomaterials Group, Centre of Macromolecular Chemistry, Ghent University, Krijgslaan 281, S4-Bis, 9000 Ghent, Belgium*
See DOI: 10.1039/x0xx00000x

amendments to the previous analytical expressions. The final model is tested against new experimental data for the photoinduced polymerization kinetics of two multiacrylate precursors along physical transformations from solid semicrystalline to solid semicrystalline and from liquid to soft rubber upon crosslinking.

Materials and methods

1.1. Materials

The photopolymerization kinetics of two acrylate end-capped urethane-based polyethylene glycol precursors (AUP) was investigated in this study. The two precursors, AUP-2 and AUP-4, were prepared following a procedure originally described by Houben et al. with PEG segments of 2000 or 4000 g mol^{-1} respectively.[25] The synthetic steps as well as the structure are schematically recalled in the supporting information SI-1. The acrylic double bond contents of AUP-2 and AUP-4, respectively 0.60 and 0.39 mmol g^{-1}, were determined experimentally by proton NMR spectroscopy.

At room temperature, the AUP's are semi-crystalline solids with crystal characteristics depending strongly on the length of the PEG segment in the backbone. After cooling from the melt to -20°C, at -5°C min^{-1}, the precursors are characterized by a melting peak at $T_m \approx 37$ and 48°C for AUP-2 and AUP-4 respectively (DSC thermograms provided in supporting information SI-2). At 60°C, the AUP-2 and AUP-4 precursors are liquid with a zero-shear viscosity of 6.7 and 24 Pa s, respectively.

With emphasis on the photoinitiation aspects, the free-radical polymerization was studied in self-initiated conditions but also upon addition of a common photoinitiator, i.e. 1-hydroxycyclohexyl phenyl ketone (HCPK, Irgacure® 184, BASF, M_w = 204.3 g mol^{-1}), at 0.5 w/w% (i.e. ≈ 28 mmol L^{-1}).

1.2. Differential photocalorimetry

Characterization of the polymerization kinetics was conducted using differential photocalorimetry at different light intensities. The DPC thermograms were recorded using a heat-flux DSC (Mettler DSC823e) equipped with a monochromatic UV-light source (UV-LED 365 nm Thorlabs) and optical light guides in quartz. The irradiance of the light emitted from the optical fibres was measured as close as possible to the position of the crucibles with a high resolution thermal power sensor from Thorlabs. Aluminum crucibles of 20 µL were used after an alkaline treatment of the surface using a solution of concentrated NaOH (0.5 M) in order to achieve a regular and reproducible wetting of the pan by the hydrophilic precursors. The sample mass was typically between 2.0 and 3.0 mg forming a layer with a thickness less than 200 µm. All measurements were conducted using dry nitrogen as inert flow gas (50 mL min^{-1}). The temperature and heat flow signal of the DSC cell (Mettler, FRS5) were calibrated using indium. The heat of polymerization of acrylate double bonds was verified from the photopolymerization of lauryl acrylate (Aldrich, 90%) up to complete conversion. A value of 79 ± 1 kJ mol^{-1} was determined in good agreement with literature.[22] This value was used throughout this work.

The duration of UV-exposure for photoreaction monitoring was typically 12 min in order to record the entire reaction exotherm. Prior to irradiation, the sample was held in the molten state at 60°C for at least 10 min under a flow of nitrogen gas to remove all dissolved oxygen, then cooled at a rate of -5 °C min^{-1} to -20°C and held in isothermal conditions for 10 min to complete crystallization. Next, photopolymerization was conducted in the solid state at 20°C. The photopolymerization of the resin was also studied in the molten state at a temperature of 60°C.

In the DPC runs the heat flow signal generated by the incident light was largely compensated upon simultaneous illumination of the reference and sample side of the cell. However, a shift of the baseline, proportional to the incident light power, was still noticed upon light exposure resulting from residual unbalance in the cell. Furthermore, the baseline level was reached with a delay owing to the instrumental response of the DSC.[26,27] As a consequence, for a reacting sample the exothermic heat flow signal from the polymerization added to the background signal thereby resulting in a step-like function. Applying the Gans-Nahman approach introduced for step-like waveforms in electronics, the polymerization exotherm could be separated from the background signal as detailed in supporting information SI-3.[28] For further kinetic analysis, the heat flow signal was scaled by the total heat of polymerization calculated from the double bond content to obtain the conversion rate R. At any time, the relative double bond conversion p was determined by partial integration of the reaction exotherm and scaling with respect to the total heat of polymerization.

Scaling model for FRP kinetics of crosslinked networks

Next to the existing literature and models related to the kinetics of free-radical polymerization,[1-11] we recently introduced a kinetic scaling model able to describe the non-steady state polymerization kinetics observed for multiacrylate precursors in solid form. In particular, the behaviour was captured in a single self-contained expression with three adjustable parameters only.[24] A key element behind the mathematical simplicity is the approximation of the structural dependence of the average kinetic coefficients for propagation and termination following scaling principles common in polymer physics.[29,30] For the propagation and bimolecular termination of the radicals involved in the non-linear chain reaction, power-law approximations in terms of the fractional conversion p were suggested to account for the structural arrest and the growing constraints in centre-of-mass and segmental diffusion, i.e.

$$k_p = k_p^0 \varepsilon^v \qquad (1)$$

$$k_t = k_{t,d}^0 \varepsilon^\mu + k_{t,rd}^0 (1-p) \varepsilon^v \qquad (2)$$

where k_p and k_t are the effective rate coefficients for propagation and bimolecular termination respectively. The latter comprises the coupling and disproportionation modes of biradical termination. While the rate coefficient of propagation is primarily controlled by the chemical coupling between a radical and a double bond over most of the polymerization, it is not true for the fast biradical termination which is chiefly controlled by diffusional processes from centre-of-mass mobility and reaction propagation, as widely documented in literature.[2,8] The diffusional contributions to the termination rate are additive and are respectively denoted as $k_{t,d}^0$ and $k_{t,rd}^0$ for translation and reaction propagation (also referred to as reaction diffusion), where the upper index 0 refers to zero conversion. Russell et al. showed that $k_{t,rd}^0 = A\boldsymbol{M}_0 k_p^0$ where A is a proportionality factor close to unity and $\boldsymbol{M}_0$ stands for the initial molar concentration of reactive functions (i.e. acrylate double bonds in the present context).[8] Similar to conventions in polymer physics, ε refers to the relative extent of reaction with the difference that it is expressed relative to the limiting conversion p_f relevant for local reaction kinetics, instead of the critical conversion germane to percolation and gel formation, i.e. $\varepsilon = 1 - (p/p_f)$.[29,30] μ and v are empirical powers describing the effect of structural changes on the kinetic coefficients. A non-zero value of v characterizes the structural cessation of the propagation process which is usually attributed to vitrification when relevant. Experimental evidence shows that k_p behaves fairly constant over most of the conversion range with a marked decrease close to the limiting conversion.[2,14,15,17] Within a good accuracy such behaviour can be approximated by eq. (1), e.g. for $v < 1$. For comparison, other semi-empirical theories for the prediction of k_p at high conversions were primarily based on the free volume concept resulting in exponential-based expressions including multiple thermal parameters, not always straightforward to assess.[11-13,16,21]

In the preceding account, the relationship between polymerization rate and conversion was established by solving the rate equations of the double bond conversion and the macromolecular chain radicals with a sink term describing the rate change related to the population of trapped ("inactive") radicals.[24] However, the kinetics of the primary radicals was not elaborated in detail and, as will appear below, allows to introduce distinctly the aspect of caging.

A free radical chain polymerization involves the formation of primary radicals $P^\bullet$ from an initiating moiety I by e.g. decomposition or hydrogen abstraction. This mechanism can be activated by e.g. heat or light.[31,32] In particular for photo-induced cleavage (photolysis) of a photo-sensitive initiator,

$$I \rightarrow 2P^\bullet \qquad (a)$$

where all primary radicals are assumed as quasi-equivalent further. According to the law of Beer-Lambert, the rate of decomposition of the initiator reads as

$$R_d(\lambda) = \varphi_d I_{0,\lambda} (1 - e^{-\alpha_\lambda})/d \qquad (3)$$

where φ_d is the quantum yield, $I_{0,\lambda}$ denotes the incident light intensity at wavelength λ, d is the depth and $\alpha_\lambda = 2.303\epsilon_\lambda[I]d$ is the absorbance with ϵ_λ the molar extinction coefficient.[31] φ_d equals the number of primary radicals that are produced for an absorbed photon taking into account various deactivation channels but also primary geminate recombination (so-called "cage effect").[1,33,34] Initiator fragments residing for a certain time in close vicinity are characterized by a recombination probability typically expressed by a factor $k_D(k_D + k_a)^{-1}$, where k_D represents the rate coefficient to diffuse away from each other and k_a is the rate

constant for geminate radical recombination.[33] Russell et al. were first to point out that the structural arrest of propagation is not necessarily the predominant mechanism to stop free radical bulk polymerization well before complete conversion.[7,9] It was shown that initiator efficiency also knows a dramatic decline as a result of structural immobilization at high conversion where primary radicals remain trapped in close proximity after initiator dissociation likely followed by geminate recombination. Data reported for the drop of initiator efficiency in terms of polymerization extent show a behaviour similar to the propagation rate and, hence, is modelled along the same lines in this work i.e. $\varphi_d = \varphi_d^0 \varepsilon^\omega$, yet with a distinct power ω.

When $\alpha_\lambda \ll 1$, i.e. the thin film approximation, eq. (3) reduces to

$$R_d(\lambda) = \varphi_d I_{0,\lambda} \alpha_\lambda / d \qquad (4).$$

With an initiator load of 0.5 w/w% of HCPK, the value of α_λ at λ = 365 nm is $\alpha_{365} \approx 0.048$ for a layer of 0.2 mm (ϵ_{365} = 37.5 L mol^{-1} cm^{-1}). It is inferred that the initiator decomposition rate is almost uniform over the entire sample. Hence, eq. 4 provides a good approximation and can be rewritten as

$$R_d = R_d^0 \varepsilon^\omega \qquad (5)$$

with $R_d^0 = K_{PI} \varphi_d^0 I_{0,365}$ and K_{PI} = 7.36 10^{-6} (mol L^{-1} s^{-1})/(mW cm^{-2}) when $I_{0,365}$ is expressed in mW cm^{-2} and R_d^0 in mol L^{-1} s^{-1}. At the highest intensities applied in the experiments of this work (≈ 100 mW cm^{-2}), an upper bound of the order of 10^{-3} mol L^{-1} s^{-1} is estimated for R_d^0.

Primary radicals can initiate the chain reaction by coupling to the functionality *M* ("monomer function"), creating the first monomer radical,

$$P^\bullet + M \rightarrow M_1^\bullet \qquad (b)$$

However, primary radicals are also susceptible for recombination with other radicals,

$$P^\bullet + M^\bullet \rightarrow PM \qquad (c)$$
$$P^\bullet + P^\bullet \rightarrow I \qquad (d)$$

where $M^\bullet$ stands for a radical of a general *M* functionality ($M^\bullet \in \{M_i^\bullet\}_{i=1\rightarrow\infty}$).[35] Mechanism *(d)* is usually designated as secondary geminate recombination of primary radicals which could escape from their initial cage after initiator decomposition.

Upon continuous photogeneration, a steady-state regime is assumed for the number of $P^\bullet$ radicals. According to mass-action kinetics, the steady-state balance for the respective rate contributions of reactions (*a*) to (*d*) can be written as

$$-R_d + (k_i \boldsymbol{M} + k_{tp} \boldsymbol{M}^\bullet)\boldsymbol{P}^\bullet + 2k_r \boldsymbol{P}^{\bullet 2} = 0$$

where bold symbols refer to molar concentrations.

The solution of the this quadratic equation provides the steady-state concentration of primary radicals. In the slow decomposition limit, $R_d \ll (k_i \boldsymbol{M} + k_{tp} \boldsymbol{M}^\bullet)^2 / 8k_r$, the solution reduces to

$$\boldsymbol{P}_s^\bullet \approx R_d / (k_i \boldsymbol{M} + k_{tp} \boldsymbol{M}^\bullet) \qquad (6)$$

whereas in the fast decomposition limit,

$$\boldsymbol{P}_s^\bullet \approx \sqrt{R_d / (2k_r)}. \qquad (7)$$

With kinetic coefficients typical for radical-monomer and radical-radical couplings, i.e. $k_i \approx k_p \approx 10^2$-$10^3$ M^{-1} s^{-1} and $k_{tp} \approx k_t \approx 10^3$-$10^4$ M^{-1} s^{-1} along with the orders of magnitude for $\boldsymbol{M} \approx 1$ M and for $\boldsymbol{M}^\bullet \approx 5\ 10^{-4}$ M (vide infra), it is anticipated that the slow decomposition limit prevails up to the end of polymerization. Eq. (6) encompasses the proportionality of the primary radical concentration and the incident light intensity which is often implicitly assumed. In contrast, eq. (7) shows that proportionality is lost in the fast decomposition regime owing to significant secondary geminate recombination.

In absence of side mechanisms, e.g. such as inhibition reactions, the rate equation for the pool of $M^\bullet$ radicals includes an initiation contribution and two biradical termination terms,

$$R_{M^\bullet} = \frac{\mathrm{d}\boldsymbol{M}^\bullet}{\mathrm{dt}} = k_i \boldsymbol{P}^\bullet \boldsymbol{M} - k_{tp} \boldsymbol{P}^\bullet \boldsymbol{M}^\bullet - 2k_t \boldsymbol{M}^\bullet \boldsymbol{M}^\bullet$$

which for $\boldsymbol{P}^\bullet = \boldsymbol{P}_s^\bullet$ in the slow decomposition limit becomes:

$$\frac{\mathrm{d}\boldsymbol{M}^\bullet}{\mathrm{dt}} = R_d \frac{k_i \boldsymbol{M} - k_{tp} \boldsymbol{M}^\bullet}{k_i \boldsymbol{M} + k_{tp} \boldsymbol{M}^\bullet} - 2k_t \boldsymbol{M}^\bullet \boldsymbol{M}^\bullet$$

or

$$R_{M^\bullet} = R_d - 2k_t \boldsymbol{M}^\bullet \boldsymbol{M}^\bullet \qquad (8)$$

as long as $k_{tp}\boldsymbol{M}^{\bullet} \ll k_i\boldsymbol{M}$. An estimate of the steady-state concentration of $M^{\bullet}$ provides a suitable order of magnitude for the upper bound of $\boldsymbol{M}^{\bullet}$. Equating eq. (8) to zero, one finds $\boldsymbol{M}_{\boldsymbol{s}}^{\bullet} = \sqrt{R_d/(2k_t)} \approx 5\ 10^{-4}$ M as upper bound using the highest R_d^0 value expected from the experimental conditions in this work. Within typical orders of magnitude for the kinetic coefficients, eq. (8) is a valid approximation and was used as the starting point in our foregoing paper.[24] Trapped $M^{\bullet}$ radicals were considered as a distinct family with no activity in the initial version of the model, as suggested in earlier papers.[19,20,36,37] The loss of active radicals due to "trapping" was taken into account by an additional sink term R_o in eq. (8). However, it is argued that the idea to consider trapped radicals as a separate pool in terms of kinetics is fundamentally unjustified. By definition, all $M^{\bullet}$ radicals formed in the course of the polymerization reaction are active. The survival time or persistence of a propagating radical before termination may extent long after the experimental time interval of kinetics monitoring, depending on its structural environment and local mobility. This explains the well-known dark or after (post) cure behaviour and the evidence of radicals with virtually infinite lifetime (trapped) but without fundamental loss of chemical activity.[38-42] It is now clear that the artificial sink term R_o in the previous description actually compensated the incorrect assumption that the initiation rate was constant over the course of the polymerization. In the present context, by virtue of eq. (5), R_d is time-dependent and vanishes at the limiting conversion which, along with the decline of k_t (eq. (2)) results in the extinction of $M^{\bullet}$ generation and termination in eq. (8). The structural changes in the course of the polymerization affect the kinetics of the reacting species (monomer functions and radicals). The interaction between kinetics and structure leads to residual unreacted monomer functions and radicals where the loosely defined term "trapped" refers to residuals with a long but unspecified lifetime. Furthermore, the usual picture that residual radicals result from a monomolecular termination mechanism is in conflict with the definition of termination itself, i.e. as a process leading to the disappearance of the radical.

Finally, the rate equation relevant to the consumption of M functions is

$$R_M = \frac{d\boldsymbol{M}}{dt} = -k_i\boldsymbol{P}^{\bullet}\boldsymbol{M} - k_p\boldsymbol{M}^{\bullet}\boldsymbol{M}$$

It is convenient to express the latter equation in terms of the fractional conversion p using $\boldsymbol{M} = \boldsymbol{M}_0(1-p)$ which then defines the polymerization rate as

$$R = \frac{dp}{dt} = -R_M/\boldsymbol{M}_0 = k_p\left(\frac{k_i}{k_p}\boldsymbol{P}^{\bullet} + \boldsymbol{M}^{\bullet}\right)(1-p)$$

This equation simplifies to

$$R = k_p\boldsymbol{M}^{\bullet}(1-p) \qquad (9)$$

when $(k_i/k_p)P^{\bullet} \ll M^{\bullet}$ which is the case for the slow decomposition limit valid here (from eq. (6) $\boldsymbol{P}_{\boldsymbol{s}}^{\bullet} < 10^{-6}$ M $\ll \boldsymbol{M}_{\boldsymbol{s}}^{\bullet}$).

As demonstrated before, the radical concentration $\boldsymbol{M}^{\bullet}$ can be solved from eqs. (8) and (9) for conversion-dependent kinetic coefficients, and subsequently substituted in eq. (9) to recover the expression for the polymerization rate R,

$$R = (1-p)\left[(R_d k_p/2\rho)\left(1-e^{-4\theta}\right)\right]^{1/2} \qquad (10)$$

with $\rho = k_t/k_p$ and

$$\theta = \int_0^p \frac{\rho(p')}{(1-p')}dp' \qquad (11)$$

with p' denoting the integration variable.[47]

Eq. (10) extents the classical steady-state approximation $R_s = (1-p)\sqrt{R_d k_p/(2\rho)}$ to non-steady-state behaviour characterized by the growth function $\phi = \sqrt{1-e^{-4\theta}}$ of the radical concentration, i.e. $\boldsymbol{M}^{\bullet} = \boldsymbol{M}_{\boldsymbol{s}}^{\bullet}\,\phi$. After solving the integral for θ using eqs. (1) and (2), eq. (10) can be transformed in the suitable parametric form

$$R = (1-p)\left[(x_1/(2\rho))\left(1-e^{-4\theta}\right)\varepsilon^{x_3}\right]^{1/2} \qquad (12)$$

with

$$\rho = x_2(1-p) + x_4\varepsilon^{x_5} \qquad (13)$$

and

$$\theta \approx x_2 p + (x_4/x_5)(1-\varepsilon^{x_5})p_f \qquad (14)$$

where $x_1 = R_d^0 k_p^0$, $x_2 = k_{t,rd}^0/k_p^0$, $x_3 = \omega + \nu$, $x_4 = k_{t,d}^0/k_p^0$ and $x_5 = \mu - \nu$. The second term in eq. (14) is an approximation holding for exponents $x_5 > 5$, typical for the fast deceleration of translational mobility at the

early stage of the polymerization. Note that when p_f = 1, the formal solution $\theta = x_2 p + (x_4/x_5)(1 - \varepsilon^{x_5})$ holds. x_1 is the single parameter that depends explicitly on the incident light intensity and is expected to behave in a proportional way. The parameters x_2 and x_4 provide respectively estimates for the kinetic termination coefficients of reaction diffusion and translational diffusion relative to the propagation coefficient at zero conversion. The decrease of polymerization rate at the end is characterized by the power x_3 which includes contributions from the decline of the initiation efficiency and from the gradual arrest of propagation.

For comparison to experimental data, the set of parameters needs to be reduced in order to achieve stable and reliable parametric estimations. In the solid-state approximation where termination by centre-of-mass diffusion can be disregarded (i.e. $k_{t,d}^0 \approx 0$), $\rho = x_2(1 - p)$ and $\theta = x_2 p$, which results in a simplification of the polymerization rate to the closed-form three-parameter function of the conversion,

$$R = [(x_1/2x_2)(1-p)(1-e^{-4x_2 p})\varepsilon^{x_3}]^{1/2} \qquad (15)$$

Another important limit, implicitly assumed in many reported studies, is steady-state where $\theta \gg 1$ and $R = (1-p)[(x_1/2\rho)\varepsilon^{x_3}]^{1/2}$. Upon transformation, a four-parameter expression can be proposed in the form

$$R = (1-p)[z_1(1-p)\varepsilon^{-z_3} + z_2\varepsilon^{z_4}]^{-1/2} \qquad (16)$$

with $z_1 = x_2/x_1$; $z_2 = x_4/x_1$; $z_3 = x_3$ and $z_4 = x_5 - x_3$. In this formulation, an inverse proportionality is predicted for the parameters z_1 and z_2 relative to the incident light intensity.

According to eq. (10), the steady-state limit is approached within 2% when $\theta \geq 1$. The mapping of the values of ρ and θ along the conversion highlights the steady-state window as illustrated in Figure 1 for fixed values of $x_2 = k_{t,rd}^0/k_p^0$ = 2 and x_5 = 20 and a variable ratio $x_4 = k_{t,d}^0/k_p^0$. From eq. (14) it is shown that $\lim_{p\to 0}\theta = (x_2 + x_4)p$ and hence $\theta = 0$ at zero conversion, consistent with zero polymerization rate ($R = 0$) at the onset of the reaction. Reaching steady-state quickly, say around 1% of conversion, requires that the condition $(x_2 + x_4)p \approx 1$ is fulfilled. Since typically $x_2 \approx 1$ to 10, this condition implies that the translational kinetic coefficient should be higher than the propagation coefficient by at least two orders of magnitude, i.e. $x_4 > 10^2$, which is usually achieved for precursors or monomers with a very low viscosity. For precursors characterized by a higher initial viscosity and slower translational mobility, $k_{t,d}^0$ is expected to be smaller, resulting in a shift to larger conversion values where steady-state is reached. In the case where reaction diffusion prevails from the start, i.e. $x_2 \gg x_4$, the build-up of the radical concentration towards steady state fully controls the acceleration of the polymerization rate up to a fractional conversion of $p \approx 1/x_2$ (0.5 in the example of Fig. 1). At the end of the polymerization, the limit $\lim_{p\to p_f}\theta = (x_2 + (x_4/x_5))p_f$ applies with a value usually exceeding one for sizeable limiting conversions.

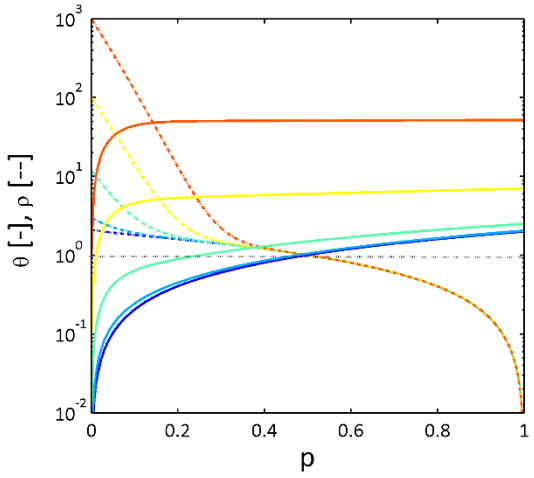

Figure 1. Plot of the ratio ρ (dashed lines, eq. (13)) and the integral θ (solid lines, eq. (14)) as a function of the fractional conversion. The curves shift from blue to red for $x_4 = k_{t,d}^0/k_p^0$ values ranging from 10^{-1} to 10^3 in logarithmic spacing with power steps of 1. The other relevant parameters have the fixed values $x_2 = k_{t,rd}^0/k_p^0$ = 2 and x_5 = 20.

2. Experimental

3. Results and discussion

The application of the present kinetic scaling model is illustrated for two acrylated urethane precursors. At 20°C, the precursors are in a solid semi-crystalline state with crystallites formed by the PEG-based backbone. It has been suggested that the acrylate double bonds, capping the precursor, concentrate along the crystalline domains forming a continuous structure. Radicals generated in the vicinity of the double bonds initiate the free-radical polymerization driven by reaction diffusion as any translational motion of the molecules is impeded. To what extent the morphology affects the polymerization kinetics is investigated here by comparing

AUP's based on PEG segments of significantly different molar mass. Using monochromatic UV-light from a LED source at 365 nm the photopolymerization was studied in well-defined activation conditions using differential photocalorimetry. After suitable correction for background and instrumental distortion, the polymerization exotherms were converted to rate-conversion profiles as shown for AUP-4 at 20°C in Figs. 2 and 3, without and with a load of additional photoinitiator respectively. Consistent with a FRP process in the "solid-state" regime, the experimental data could successfully be compared to eq. (15) after adjustment of the three parameters in the non-linear least-squares sense as reported previously. The single parameter with an explicit dependence of the incident light intensity is $x_1 = R_d^0 k_p^0$. A linear behaviour with slope one is predicted in a double logarithmic representation according to $\log(x_1) = \log\left(K\varphi_d^0 k_p^0\right) + \log(I_{0,365})$. Plots of the adjusted parameters against the incident light intensity are presented in Fig. 4 for a large body of photopolymerization experiments conducted for the two precursors as such and after addition of 0.5 w/w% of HCPK photoinitiator. The double logarithmic plots of the parameter x_1 in Fig. 4a demonstrate the expected linear behaviour with a slope close to one as evaluated from a linear regression of $\log(x_1) = a\log(I_{0,365}) + b$, with a and b values listed in Table 1. Whereas the lines are almost overlapping for the kinetic experiments with additional photoinitiator, there is a clear enhancement for AUP-4 relative to AUP-2 in the self-initiation case, suggesting some effect related to the crystalline morphology. With K known, an upper bound for k_p^0 can be provided from $k_p^0 = 10^b/K$ using $\varphi_d^0 = 1$. However, without external photoinitiator K (denoted as K_a) cannot be estimated a priori. Upon the "standard" addition of an external PI and following an additive rule, K reads as $K = K_a + K_{PI}$ with the value K_{PI} = 7.36 (10^{-6} mol L^{-1} s^{-1})/(mW cm^{-2}) calculated before in the assumption that the photoinitiator remains uniformly distributed over the sample after solidification. By combining the two results, one then estimates $k_p^0 = (10^{b_{PI}} - 10^{b_a})/K_{PI}$ from the intercept values b_{PI} and b_a reported in Table 1. Accordingly, the estimated values of k_p^0 are 200 ± 30 and 160 ± 30 L mol^{-1} s^{-1} for AUP-2 and AUP-4 respectively, in good agreement with the order of magnitude cited in earlier reference papers.[14-17,48] Likewise, the factor K_a can next be obtained as $K_a = 10^{b_a}/k_p^0$ and K_a = 1.1 ± 0.3 and 3.6 ± 0.8 (10^{-6} mol L^{-1} s^{-1})/(mW cm^{-2}) for AUP-2 and AUP-4 respectively. The outcome shows a significant contribution of self-initiation in the semi-crystalline state with an efficiency that depends on the morphological details. The physico-chemical mechanism behind self-initiation is not yet understood but clearly gains effectiveness when double bond packing is improved. Along the same lines, self-initiation becomes insignificant for disordered melts of the precursors.[24] The second parameter of interest is x_2 which provides a straightforward indication for the ratio between the kinetic coefficients of termination by reaction diffusion and propagation, $x_2 = k_{t,rd}^0/k_p^0$. Expectedly, this ratio appears as independent of the light intensity in Fig. 4b but reflects some sensitivity towards structural factors, as suggested by the average values reported in Table 1. The thermograms in Fig. SI-2 reveal a significant difference between the semicrystalline properties of the AUP's which are also modified to some extent after addition of the photoinitiator. In particular, the degree of crystallinity reduced significantly for AUP-4 as inferred from the decrease in the fusion enthalpy from 93 to 72 J g^{-1} getting closer to the enthalpies of AUP-2 around 63 J g^{-1} in both cases. With the differences in fusion characteristics, there is some evidence that an enhanced degree of crystallinity (cf. AUP-4) and the concomitant morphology likely explain an acceleration of the reaction diffusion process and an increased self-initiation efficiency as noticed before. Theoretical investigations addressing residual termination by reaction diffusion have shown that the ratio $k_{t,rd}^0/k_p^0 = A\boldsymbol{M}_0$.[4,5,8] A packing effect of the double bonds owing the crystal formation potentially increases the local double bond concentration, $\boldsymbol{M}_0$, but also the interaction volume expressed by the factor A.

The curvature of the rate-conversion profile at the end of the polymerization determines basically the power x_3 which quantifies empirically the decline of the initiation and the propagation efficiency, within the validity conditions of the outlined model. In particular, the slow decomposition limit and the condition $k_{tp}\boldsymbol{M}^{\bullet} \ll k_i\boldsymbol{M}$ justifying the use of eq. (8) may start to fail at high conversions. With limiting conversions in the range 0.4-0.7 (Figs. 2, 3 and SI-4), this is not really compromised here. A weak increasing trend appears for all datasets plotted as a function of the incident light intensity in Figure 4c. The average values of x_3 in Table 1 are also higher when an additional load of photoinitiator is added. All tend to indicate that the power $x_3 = \omega + \nu$ increases with the generation rate of primary radicals which primarily suggests an enhancement of the cage effect (ω).

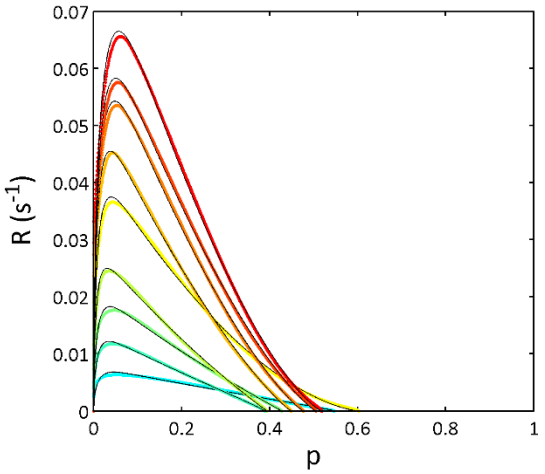

Figure 2. Rate-conversion profiles upon photopolymerization of AUP-4 at 20°C after crystallization of the precursor. The color sequence from blue to red refers to a selection of experiments conducted at increasing incident light intensities ranging from increasing from 1.6 to 114 mW cm^{-2}. The black lines result from a NLLS comparison of eq. (15) to the experimental data.

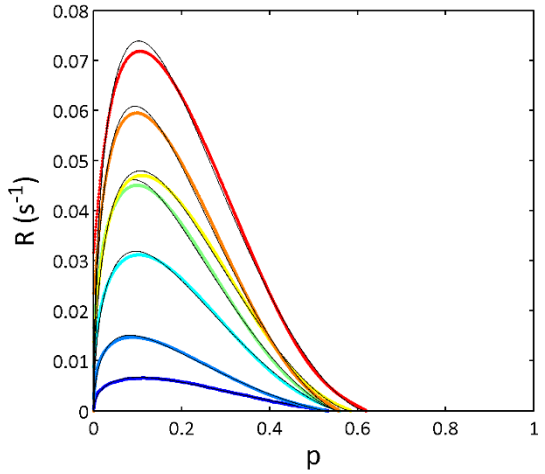

Figure 3. Rate-conversion profiles upon photopolymerization of AUP-4 in the presence of 0.5 w/w% photoinitiator at 20°C after crystallization of the precursor. The color sequence from blue to red refers to a selection of experiments conducted at increasing incident light intensities ranging from increasing from 0.2 to 12 mW cm^{-2}.. The black lines result from a NLLS comparison of eq. (15) to the experimental data.

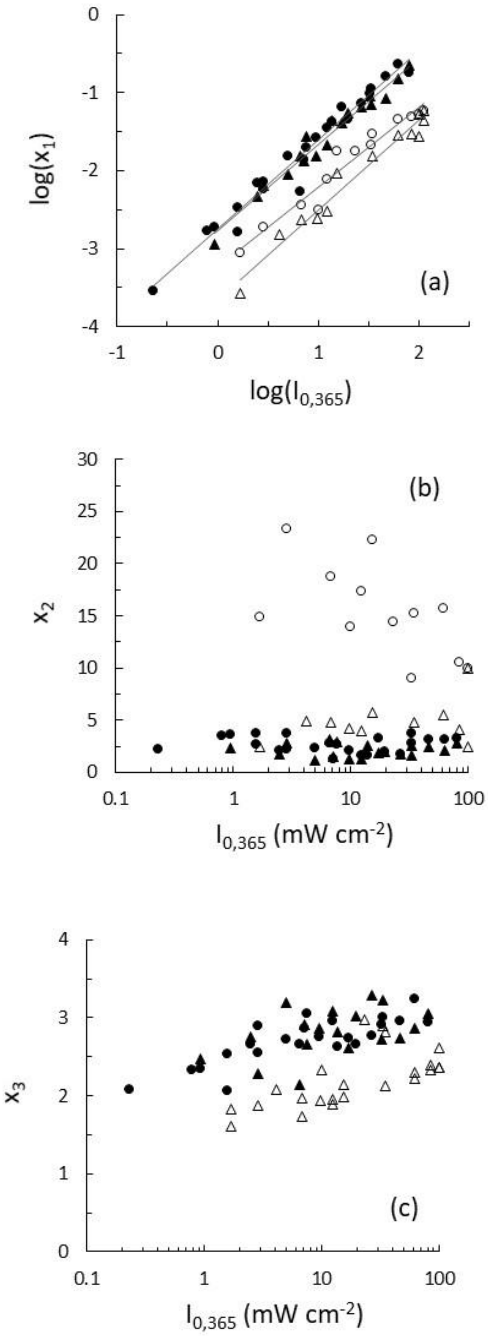

Figure 4. Plot of the adjusted parameters x_1 (a), x_2 (b) and x_3 (c) as a function of the incident light intensity at 365 nm after NLLS comparison of eq. (15) to the experimental data at 20°C. The limiting conversion at the end of polymerization is plotted in SI-4. The open and solid symbols refer to the photopolymerization kinetics in the absence of and with additional PI, respectively, with triangles for AUP-2 and circles for AUP-4. The fit errors are always smaller than the symbol size.

Table 1. Linear regression results of $\log(x_1)$ and average values of x_2 and x_3 after NLLS adjustment of eq. (15) to the

experimental rate-conversion data of the solid precursors at 20°C.

	$\log(x_1)$		$\overline{x_2}$	$\overline{x_3}$
	a	b		
AUP-2	1.15±0.07	-3.66 ±0.10	5±2	2.2±0.3
AUP-2/PI	1.10±0.05	-2.77 ±0.06	2.1±0.6	2.8±0.3
AUP-4	1.02±0.07	-3.24 ±0.10	15±5	2.3±0.4
AUP-4/PI	1.14±0.05	-2.76 ±0.05	2.7±0.8	2.7±0.3

As a second application of the kinetic scaling model, the photopolymerization kinetics was investigated for the same AUP precursors in the molten state at 60°C. Similar to previous findings, there is no signification polymerization without the addition of external photoinitiator. In Fig. 5, the polymerization rate is plotted as a function of the fractional conversion for the AUP-4 precursor with 0.5 w/w% of HCPK at incident light intensities increasing from 1.6 to 80 mW cm^{-2}. At the highest intensities, the polymerization rate seems to be finite at zero conversion typical for an instant jump to the steady-state regime. However, with the required signal correction, high-frequency filtering takes place which truncates the heat flow signal in the first fractions of a second and introduces some uncertainty for fast polymerizations, as in the present case. For viscous liquids, it is a prerequisite to verify whether the steady-state approximation holds or not. Biradical termination controlled by translational diffusion has been modelled along different lines suggesting relations of the form $k_{t,d}^0 \div \eta^{-z}$ with $z \approx 1$ when diffusion control predominates.[2,5,6,17] In order to capture the order of magnitudes, the value $k_{t,d}^0 \approx 10^6$ L mol^{-1} s^{-1} is taken from the literature as a reasonable estimate for a monomer of low viscosity ≈10 mPa s.[12-16,20,43-45] With viscosities of 6.7 and 24 Pa s, one roughly estimates $k_{t,d}^0 \approx 1500$ and 400 L mol^{-1} s^{-1} for AUP-2 and AUP-4 respectively. With a suitable guess for k_p^0, $x_4 = k_{t,d}^0/k_p^0$ can then be fixed in the fitting procedure of the model. Values between 10^2 and 10^4 mol L^{-1} s^{-1} were tested and a consistent picture appears when the value $x_4 \approx 1$ is adopted in the NLLS comparison of eq. (12), along with eqs. (13) and (14), to the rate-conversion data of the two precursors (black lines in Fig. 5). The results of the four adjustable parameters x_1, x_2, x_3 and x_5 are shown in Fig. 6a-d as a function of the incident light intensity. The parameters *a* and *b* resulting from a linear regression of x_1 in a log-log representation are summarized in Table 2, as well as the mean values of x_2, x_3 and x_5. Again, the slope *a* is in good agreement with the predicted first-order scaling for x_1 relative to the incident light intensity. The homogeneous character of the liquid precursors in the melt dilutes the self-initiation efficiency to the point that it can be neglected. Hence from the intercept *b*, one then obtains $k_p^0 = 10^{b_{PI}} / K_{PI} \approx 1200$ and 540 mol L^{-1} s^{-1} for AUP-2 and AUP-4 at 60°C respectively. Observing that the intercept is fairly insensitive to the assumed value of k_p^0, it is clear that $x_4 \approx 1$ offers a consistent input value in this case. With reference to Fig. 1, θ for $x_4 = 1$ is represented by the light blue line for comparable parameter values and suggests a non-steady behaviour over a significant conversion range. Numerous rate-conversion profiles published in the literature for the free-radical polymerization of viscous and complex liquids exhibit shapes which are reminiscent of a non-steady acceleration step as illustrated here.[10,12-16,20,46] While the macroscopic viscosity is a helpful indicator to verify the validity of the steady-state approximation for homogeneous liquids, it is inappropriate in heterogenous media where the relevant local functional mobility can differ significantly from the overall fluid properties.

At 60°C, the kinetic coefficient for propagation, k_p^0, is about 4 to 6 times higher than the value found at 20°C, in line with the results from the previous temperature study.[24] The AUP precursors transform from homogenous viscous liquids to rubbers upon polymerization at 60°C, in contrast to the solid-solid transformation at 20°C where translational motion is completely inhibited. However, the balance $k_{t,rd}^0/k_p^0$ quantified by x_2, and the scale factor at the end of the polymerization, x_3, are very similar as concluded from the mean values in Tables 1 and 2. For the homogeneous precursor melts, the proportionality factor A of the bimolecular termination process by reaction diffusion ranges between 4 and 9 as estimated from $x_2 = A\boldsymbol{M}_0$ using the average acrylate double bond concentrations determined by proton NMR

In the semi-crystalline state, the photopolymerization is proceeding in a confined amorphous space with a lack of motional freedom. Growing structural hindering will ultimately stop the progress of the reaction, akin to vitrification and characterized independently by the power contributions ω and ν in x_3 for initiation and propagation respectively. In contrast, there is no vitrification at 60°C and the parameter x_3 seems fully defined by ω which is related to the loss of initiator efficiency. In Fig. 5, the curvature of the tail of the profiles decreases at higher intensities as reflected by a decrease of the x_3 parameter in Fig. 6c but the trend is still open to discussion. The scaling power x_5 is indicative of the immobilization of radicals on the growing structures and characterizes the gel effect. Owing to the high precursor viscosity and the importance of the transient effect here, this parameter shows a strong correlation with the input value of x_4. This highlights the issue to unravel the transient behaviour from the structural kinetic effects driving the acceleration in the free-radical polymerization.

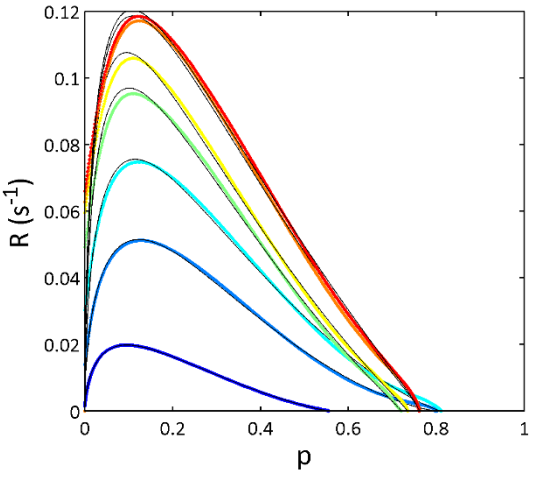

Figure 5. Rate-conversion profiles upon photopolymerization of AUP-4 containing 0.5w/w% photoinitiator at 60°C (initial melt state). The color sequence from blue to red refers to a selection of experiments conducted at increasing incident light intensities increasing from 1.6 to 80 mW cm^{-2}. The black lines result from a NLLS comparison of eq. (12) to the experimental data.

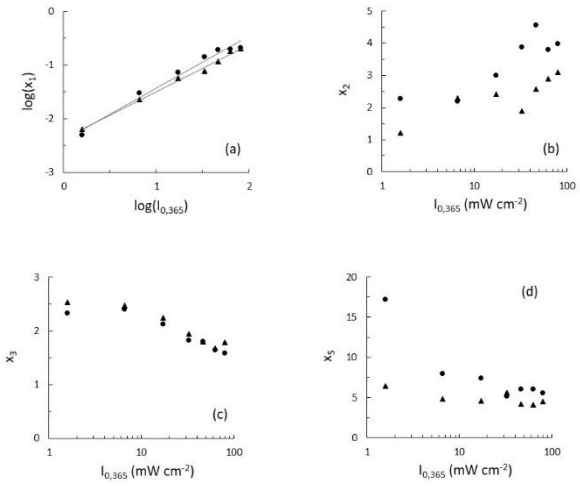

Figure 6. Plot of the adjusted parameters x_1 (a), x_2 (b), x_3 (c) and x_5 (d) as a function of the incident light intensity at 365 nm after NLLS comparison of eq. (12) to the experimental data. The limiting conversion at the end of polymerization is plotted in SI-3. The triangles and circles refer to the photopolymerization kinetics of AUP-2 and AUP-4 respectively.

Table 2. Linear regression results of $\log(x_1)$ and average values of x_2, x_3 and x_5 after NLLS adjustment of eq. (12) to the experimental rate-conversion data of the molten precursors at 60°C. x_4 was fixed to the value 1 for AUP-2 and AUP-4 respectively, as explained in the text.

	$\log(x_1)$		$\overline{x_2}$	$\overline{x_3}$	$\overline{x_5}$
	a	*b*			
AUP-2/PI	0.89 ±0.03	-2.06 ±0.05	2.4 ±0.6	2.1 ±0.3	4.9 ±0.8
AUP-4/PI	0.98 ±0.07	-2.40 ±0.10	3.4 ±0.9	2.0 ±0.3	7.9 ±4.2

Conclusions

The non-steady kinetic scaling model introduced previously to describe the kinetics of the photoinduced free-radical polymerization of crosslinking precursors has been elaborated in full detail. When primary radical generation is slow, and with the use of power-law approximations for the structurally dependent kinetic coefficients of propagation and termination, a non-steady state expression of the polymerization rate has been derived in terms of the relative functional conversion. The cage effect of primary radicals and the evidence of trapped radicals are now clearly specified. The complete rate-conversion expression can be written in a self-contained form with five adjustable parameters, having an a priori physico-chemical ground. For the situation where center-of-mass diffusion can be neglected or in the case of steady state, closed-form expressions with three and four adjustable parameters, respectively, are now available which can be used for straight comparison to experimental data of the polymerization kinetics. In particular, from a comparison of the kinetic scaling model to a large body of experimental data for acrylated urethane precursors in the semi-crystalline state, the trends predicted for the three parameters as a function of the incident light intensity have been clearly established and illustrates the strength of the approach to obtain sound kinetic factors in a quantitative way. Furthermore, in well-controlled initiation conditions, estimates for the kinetic coefficients of propagation and termination of the free-radical reaction process can be determined. A successful application of the model was also illustrated for a viscous melt of the acrylated urethane precursors, revealing that non-steady behaviour essentially drives the acceleration step of the polymerization rate. This work shows that besides the "gel" or "Trommsdorff-Norrish" effect, transient non-steady state effects should be considered on an equal footing to rationalize the rate acceleration in the free-radical polymerization of crosslinking precursors.

Conflicts of interest

There are no conflicts to declare.

Acknowledgements

We are grateful to Prof. Dr. Ir. Rik Pintelon (ELEC, Vrije Universiteit Brussel, Brussels) for his valuable advice in the analysis of the DSC signals from an electrical engineering perspective.

Notes and references

1 P.E.M. Allen and C.R. Patrick, Kinetics and Mechanisms of Polymerization Reactions. Application of Physico-Chemical Principles, John Wiley and Sons, Chichester, 1974.
2 D.S. Achilias, *Macromol. Theory Simul.*, 2007, **16**, 319.
3 C. Barner-Kowollik and G.T. Russell, *Prog. Polym. Sci.*, 2009, **34**, 1211.
4 S.K. Soh and D.C. Sundberg, *J. Polym. Sci., Part A: Polym. Chem.*, 1982, **20**, 1345.
5 M. Buback, *Makromol. Chem.*, 1990, **191**, 1575.
6 M. Buback, B. Huckestein and G. T. Russell, *Macromol. Chem. Phys.*, 1994, **195**, 539.
7 M.J. Ballard, D.H. Napper, R.G. Gilbert, D.F. Sangster and *J. Polym. Sci. Polym. Chem. Ed.*, 1986, **24**, 1027.
8 G.T. Russell, D.H. Napper and R.G. Gilbert, *Macromolecules*, 1988, **21**, 2133.
9 G.T. Russell, D.H. Napper and R.G. Gilbert, *Macromolecules*, 1988, **21**, 2141.
10 M. Stickler, *Makromol. Chem.*, 1983, **184**, 2563.
11 C.N. Bowman and N.A. Peppas, Macromolecules, 1991, **24**, 1914.
12 W.D. Cook, *Polymer*, 1992, **33**, 2152.
13 G.L. Batch and C.W. Macosko, *J. Appl. Polym. Sci.*, 1992, **44**, 1711.
14 K.S. Anseth, C.M. Wang and C.N. Bowman, *Macromolecules*, 1994, **27**, 650.
15 K.S. Anseth, C.M. Wang and C.N. Bowman, *Polymer*, 1994, **35**, 3243.
16 M.D. Goodner, C.N. Bowman, *Macromolecules*, 1999, **32**, 6552.
17 G. A. O'Neil and J. M. Torkelson, *Macromolecules*, 1999, **32**, 411.
18 C. N. Bowman and C. J. Kloxin, *AIChE Journal*, 2008, **54**, 2775.
19 E. Andrzejewska, *Prog. Polym. Sci.*, 2001, **26**, 605.
20 E. Andrzejewska, in Three-Dimensional Microfabrication Using Two-photon Polymerization, ed. T. Baldacchini, William Andrew Publishing, Norwich, 2016, Ch.2, 62.
21 P.D. Iedema, V. Schamböck, H. Boonen, J. Koskamp, S. Schellekens and R. Willemse, *Chem. Eng. Sci.*, 2018, **176**, 491.
22 C. Dworak, S. Kopeinig, H. Hoffmann and R. Liska, *J. Polym. Sci. A Polym. Chem.*, 2009, **47**, 392.
23 C. Dworak, T. Koch, F. Varga and R. Liska, *J. Polym. Sci. A Polym. Chem.*, 2010, **48**, 2916.
24 P. Roose, A. Houben, H. Van den Bergen, D. Bontinck and S. van Vlierberghe, *Macromolecules*, 2018, **51**, 5027.
25 A. Houben, P. Roose, H. Van den Bergen, H. Declercq, J. Van Hoorick, P. Gruber, A. Ovsianikov, D. Bontinck, S. Van Vlierberghe and P. Dubruel, *Materials Today Chemistry*, 2017, **4**, 84.
26 D. Pananakis and E. W. Abel, *Thermochim. Acta*, 1998, **315**, 107.
27 A. Bányász, E. Keszei, *J. Phys. Chem. A*, 2006, **110**, 6192.
28 W. L. Gans and N. S. Nahman, *IEEE Trans. Instrum. Meas.*, 1982, **31**, 97.
29 M. Rubinstein and R.H. Colby, Polymer Physics, Oxford University Press, Oxford, 2003.
30 P.-G. De Gennes, Scaling Concepts in Polymer Physics, Cornell University Press, Ithaca, NY, 1979.
31 J.P. Fouassier, Photoinitiation, Photopolymerization, Photocuring, Hanser, Munich, 1995.
32 S. P. Pappas, UV-Curing: Science and Technology, Technology Marketing Corp., Stamford CT, 1986; Plenum Press, New York, 1992.
33 D.L. Kurdikar and N.A. Peppas, *Macromolecules*, 1994, **27**, 733.
34 I. Khudyakov, A.A. Zharikov and A.I. Burshtein, *J. Chem. Phys.*, 2010, **132**, 014104.
35 P.J. Flory, Principles of Polymer Chemistry, Cornell University Press, Ithaca, NY, 1953.
36 M. Wen and A.V. McCormick, *Macromolecules*, 2000, **33**, 9247.
37 A. Ibrahim, V. Maurin, C. Ley, X. Allonas, C. Croutxé-Barghorn, F. Jasinski, *Eur. Polym. J.*, 2012, **48**, 1475.
38 J.G. Kloosterboer, G.M.M. van de Hei, R.G. Gossink and G.C.M. Dortant, *Polym. Comm.*, 1984, **25**, 322.
39 J.G. Kloosterboer, G. F.C.M. Lijten and F.J.A.M. Greidanus, *Polym. Commun.*, 1986, **27**, 268.
40 C. Decker and K. Moussa, *J. Polym. Sci. Polym. Chem. Ed.*, 1987, **25**, 739.
41 S. Zhu, Y. Tian, A.E. Hamielec and D.R. Eaton, *Polymer*, 1990, **23**, 1144.
42 S. Zhu, Y. Tian, A.E. Hamielec and D.R. Eaton, *Polymer*, 1990, **31**, 154.
43 C. Barner-Kowollik, F. Bennet, M. Schneider-Baumann, D. Voll, T. Rölle, T. Fäcke, M-S. Weiser, F-K. Bruder and T. Junkers, *Polym. Chem.*, 2010, **1**, 470.
44 S. Beuermann and M. Buback, *Prog. Polym. Sci.*, 2002, **27**, 191.
45 K. Liang and R.A. Hutchinson, *Macromol. Rapid. Commun.*, 2011, **32**, 1090.
46 K.S. Worthington, C. Baguenard, C., B.S. Forney, C.A. Guymon, *J. Polym. Sci. Part B: Polym. Phys.*, 2017, **55**, 471.
47 The upper limit of the integral was misprinted in eq. (10) of ref. 23.
48 In ref 23, a rough guess of the order of 10^4 was improperly estimated for k_p^0 of AUP-2 by overlooking the full spectral content of the polychromatic mercury source. With an appropriate summation of the decomposition rates over the

spectral range of the UV light, the new estimate of k_p^0 is around 400 L mol^{-1} s^{-1}, closer to the values reported here.